Nanoreactors

Size Tuning, Functionalization, and Reactivation of Au in TiO_2 Nanoreactors**

*Jing Li and Hua Chun Zeng**

Over the past few years, there have been a significant number of new methods developed for the fabrication of core–shell structures ranging from multiphase semiconductors to metal–metal oxide nanocomposites.[1–10] Recently, the engineering of movable cores inside hollow shells has also been achieved with a silica template method and a Kirkendall-type diffusion process.[6,10] If the shell is permeable to reactants, this new type of core–shell nanostructure can be considered in a wider sense as a tiny reactor containing a movable catalyst core. As regards their applications, hydrogenation of ethylene (C_2H_4) has been conducted in Pt–CoO hollow core–shell nanostructures, and the heterogeneous catalytic activity of Pt cores has been demonstrated in the gas phase.[10] To carry out a

[*] J. Li, Prof. Dr. H. C. Zeng
Department of Chemical and Biomolecular Engineering
Faculty of Engineering
National University of Singapore
10 Kent Ridge Crescent, Singapore 119260 (Singapore)
Fax: (+65)6779-1936
E-mail: chezhc@nus.edu.sg

[**] The authors gratefully acknowledge the financial support of the Ministry of Education, Singapore.

Supporting information for this article is available on the WWW under http://www.angewandte.org or from the author.

  DOI: 10.1002/ange.200500394

wider range of chemical reactions under both gaseous and liquid conditions, we note that multifunctional core–shell nanoreactors may be required in this emerging area of research. Apart from its normal role of container, for instance, a reactor (shell) itself should also be able to participate in certain chemical processes. Furthermore, a synthetic flexibility in size manipulation, functionalization, and reactivation of the catalyst (core) in a confined environment is yet to be demonstrated. Herein, we report that hollow Au–TiO_2 core–shell nanocomposites can be synthesized by using a wet chemical approach. Encouragingly, our synthetic method offers the flexibility to investigate the aforementioned exploratory subjects. In addition to the synthetic fabrication of Au–TiO_2 nanostructures, the photocatalytic activity of the core–shell nanoreactors was elucidated by desorption and/or decomposition of anchored organic molecules on the metallic cores under UV irradiation.

To test the above conceptual schemes, we conducted a series of experiments. The schematic flowchart in Figure 1

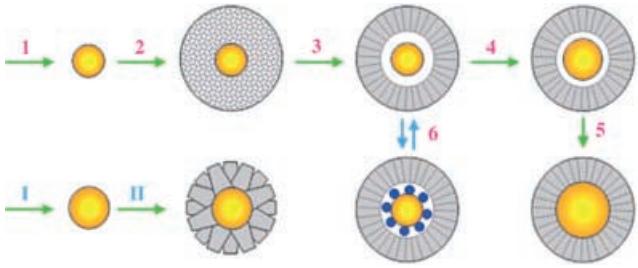

Figure 1. Schematic illustration of the three different processes investigated: fabrication of Au–TiO_2 nanoreactor and size tuning of core catalyst (steps 1–5); preparation of flowerlike Au–TiO_2 core–shell structure (steps I and II); and inclusion/removal of ionic or molecular species in an Au–TiO_2 nanoreactor (reversible steps 6). Gold cores are represented in orange/yellow, anatase TiO_2 shells in gray, and surface-anchored species in blue. Projected lines in products of steps 3–6 indicate the channels formed perpendicularly to the central space of the reactor.

illustrates some major process steps in aqueous media: 1) formation of metallic cores; 2) aggregation of TiO_2 nanocrystallites around a single metallic core; 3) evacuation of central TiO_2 crystallites by Ostwald ripening; and 4) and 5) manipulation of the metal core (that is, growth of the inside metal) to a desired size.

Figure 2 shows TEM images of the Au–TiO_2 nanoreactors fabricated through steps 1–3. For each discrete Au–TiO_2 core–shell structure, the Au catalyst core (50–150 nm) and a hollow interior can be clearly observed. The crystallites located in the central part of the TiO_2 spheres were removed during the synthesis.[11] Thus, it is understandable that intercrystallite channels must exist between the inner and outer spaces, through which ionic and/or molecular species can be transferred into or out of the nanoreactor. In addition to adjustable shell thickness and void volume through Ostwald ripening,[11,12] the size of the catalytic core can be further tuned within the nanoreactor (steps 3 and 4). In such a size manipulation, gold nutrients ($HAuCl_4$; see the Supporting Information) were first introduced into the vacant space

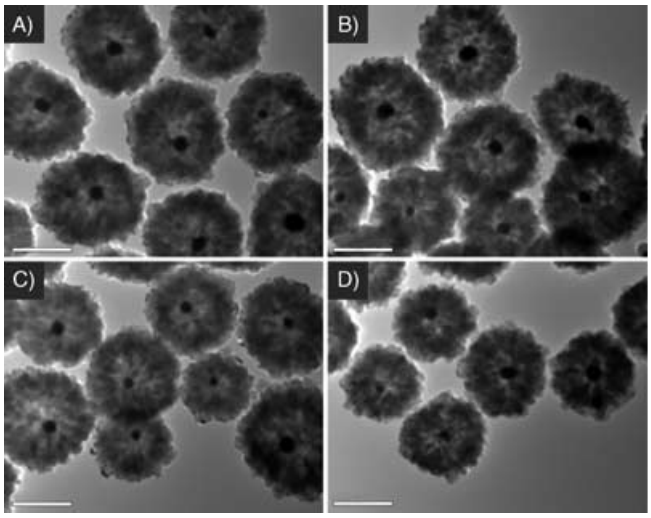

Figure 2. A)–D) TEM images of Au–TiO_2 core–shell nanoreactors with a central vacant space (prepared in step 3 of Figure 1). Experimental conditions: $HAuCl_4$ (3.1 mL, 0.32 mM) + sodium citrate solution (0.1 mL, 0.01 M) + TiF_4 (2.0 mL, 0.04 M) + H_2O to a total volume of 30.0 mL; at 180 °C for 48 h. All bar scales: 500 nm.

of the nanoreactor, and the $HAuCl_4$-soaked Au–TiO_2 nanoreactors were then placed in a solution of cetyltrimethylammonium bromide (CTAB) and ascorbic acid. It is believed that a slow interdiffusion between the $HAuCl_4$ inside the nanoreactor and the CTAB/ascorbic acid solution outside the nanoreactor would ensure a slow growth of Au cores while preventing TiO_2 shells from direct metal deposition. Furthermore, with the introduction of CTAB surfactant better-faceted Au cores can also be attained. Figure 3 shows Au–TiO_2 nanoreactors after core enlargement (Au: 150–250 nm). If $HAuCl_4$ and CTAB/ascorbic acid were premixed in the outside bulk solution, however, small Au nanoparticles would also be deposited on the outer surface of TiO_2 in addition to

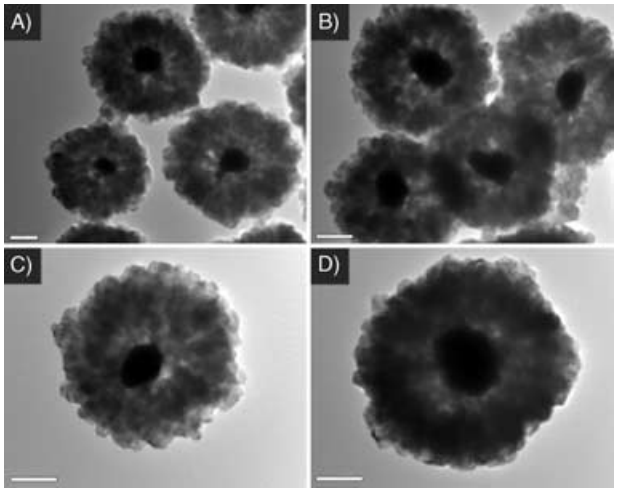

Figure 3. A)–D) TEM images of Au–TiO_2 core–shell nanoreactors after enlargement of Au cores (prepared in step 4 of Figure 1). A size-tuning experiment was carried out (see the Supporting Information); the pristine Au–TiO_2 core–shell nanoreactors used in this core tuning were those of Figure 2. All bar scales: 200 nm.

the desired core growth. In such a case, the vacant space can be filled up entirely (step 5, Figure 1; see the Supporting Information), which once again confirms the availability of communicable channels between the interior space of reactors and the exterior environment.

X-ray diffraction (XRD) investigations show that all the prepared Au–TiO_2 composite samples contain both face-centered cubic Au (space group (SG): $Fm\bar{3}m$, $a_0 = 4.078$ Å, JCPDS card No. 4-0784; see the Supporting Information) and tetragonal anatase TiO_2 (SG: $I4_1/amd$, $a_0 = 3.7852$ Å and $c_0 = 9.5139$ Å, JCPDS card No. 21-1272; see the Supporting Information). The chemical compositions of these metal–metal oxide nanocomposites were further confirmed by energy-dispersive X-ray spectroscopy (EDX). It was clearly shown that the content of Au in the size-tuned Au–TiO_2 nanoreactors increased in accordance with the enlargement of the Au cores, as evidenced in EDX elemental profiles (see the Supporting Information).

The present approach also permits other types of synthetic architecture. For example, on adding ascorbic acid to the synthesis mixture, well-faceted and much larger anatase TiO_2 crystallites were formed, which gave rise to a flowerlike Au–TiO_2 core–shell structure (steps I and II, Figure 1; see the Supporting Information). As detailed in Figure 4, the TiO_2 shell comprises only a small number of crystallites that are single-crystalline and elongated along the ⟨001⟩ directions.[11] In this case, it is likely that the ascorbic acid molecules would adsorb preferentially on certain crystal planes of TiO_2 crystallites during hydrothermal Ostwald ripening, thus resulting in larger building blocks from which the TiO_2 shell is formed. Nonetheless, this type of metal–metal oxide nanocomposite would be still very useful for new applications, such as storage of photogenerated electrons where no interior space is required.[13]

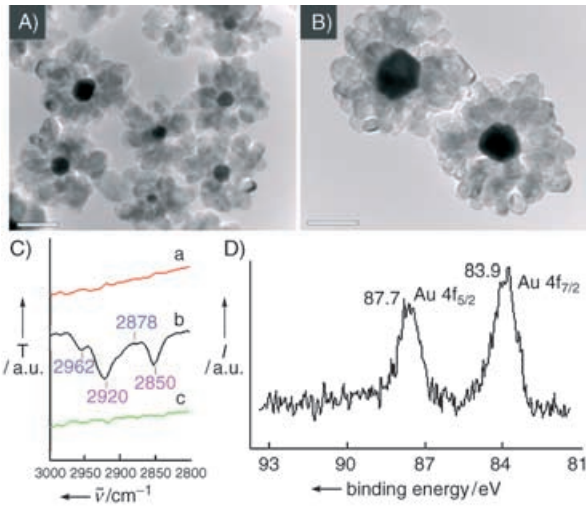

Figure 4. A, B) TEM images of flowerlike Au–TiO_2 core–shell structures (prepared in step II of Figure 1, see the Supporting Information); bar scales: 100 nm. C) FTIR spectra: a: clean Au–TiO_2; b: $C_{12}H_{25}SH$-adsorbed Au–TiO_2; and c: removal of $C_{12}H_{25}SH$ from b under UV irradiation. D) XPS spectrum of Au 4f measured for the Au–TiO_2 core–shell nanoreactors (Figure 2) after photocatalytic decomposition/desorption of adsorbed $C_{12}H_{25}SH$ molecules.

The catalytic Au cores can still be functionalized to meet targeted applications. For example, surface hydrophobicity or hydrophilicity can be attained by the introduction of alkane chains or carboxylic groups, respectively, to the Au core. Here, as a simple illustration, the straight-chain aliphatic thiol $C_{12}H_{25}SH$ was anchored on the Au surface (reversible steps 6, Figure 1). The Fourier-transform infrared (FTIR) spectra of Figure 4C show that the asymmetric and symmetric vibrational modes of C–H are located at 2920 and 2850 cm^{-1} ($\nu_{as}(CH_2)$ and $\nu_s(CH_2)$) and weaker modes at 2962 and 2878 cm^{-1} ($\nu_{as}(CH_3)$ and $\nu_s(CH_3)$), respectively, in the $C_{12}H_{25}SH$ adsorbed samples (see the Supporting Information), which indicates an all-*trans* conformation for the molecules.[14] Interestingly, after UV irradiation ($\lambda = 254$ nm, 15 h) the thiolate anions were desorbed and/or decomposed, as confirmed with both FTIR (Figure 4C) and X-ray photoelectron spectroscopy (XPS; see the Supporting Information). The Au^0 (binding energies at 87.7 and 83.9 eV, Au $4f_{5/2}$ and $4f_{7/2}$; Figure 4D) and TiO_2 (binding energies at 464.1 and 458.4 eV, Ti $2p_{1/2}$ and $2p_{3/2}$; see the Supporting Information) phases are clearly observed, whereas the signals for S over the binding energy range 160.0–170.0 eV are absent (see the Supporting Information).[14,15] This XPS observation indicates that the Au cores became clean again after removal of the anchored thiolate anions. In this process, the photogenerated holes in the valance band are likely to be responsible for the organic molecular oxidation (including the solvent used, ethanol;[16] see the Supporting Information), whereas the photogenerated electrons may transfer to the metallic core and induce reductive desorption of anionic sulfur species ($-S^{\delta-}$) from the Au surface. The reversibility of this process could be very useful for sulfur-poisoned metal catalyst regeneration in actual applications. It should also be recognized that unlike the normal Au–oxide nanocomposites (for example, Au–TiO_2) reported in literature,[17] the composite nanoreactors fabricated in the present work possess an additional function of screening reactants as a result of the presence of membrane-like shells. With this new structural feature (that is, inorganic membrane reactors), only chemical species permeable through the shell channels can access the catalytic metal cores and thus undergo metal-catalyzed reactions. In this regard, effective control of pore structure and channel size as well as chemical modification (inorganic and/or organic anchoring) of channel walls for the reactor shells would become immediate research tasks in future selective reactions. To further develop the nanoreactors, it is anticipated that higher catalytic activity could be attained with even smaller metal nanoparticles. Current research efforts are directed toward the size reduction of the reactor as well as chemical compatibility between the prepared solid materials (reactors) and solution constituents (reactants, products, and solvent media which form the reaction environment), although further exploitation appears to be challenging.

In summary, the preparation, size manipulation, functionalization, photocatalytic reactions, and reactivation of gold nanoparticles inside Au–TiO_2 nanoreactors have been dem-

onstrated. The current approach offers a method for the synthetic fabrication of complex nanocomposites with high process flexibility. Many other catalytic reactions, in both the gaseous and liquid phase, can be conducted in this type of photosensitized metal–semiconductor nanoreactor. It is believed that higher catalytic activity and selectivity can be achieved when metal cores are trimmed down to even smaller sizes and the channel structure of the shell is better controlled.

Experimental Section

The synthesis of Au–TiO_2 core–shell nanoreactors involves a number of process steps (Figure 1). For the preparation of the starting Au-core nanoparticles, $HAuCl_4$ (3.0–4.0 mL, 0.2–0.6 mM) was mixed with sodium citrate solution (0.075–0.40 mL, 0.01M). After the solution was stirred for 3–4 h at room temperature (that is, after forming Au-seed nanoparticles, step 1, Figure 1), TiF_4 (1.0–2.0 mL, 0.04 M) and deionized water were added sequentially to a total volume of 30.0 mL. The mixture was then transferred to a Teflon-lined stainless-steel autoclave, and the hydrothermal reaction was conducted at 180 °C for 48 h in an electric oven. During this process, anatase TiO_2 crystallites were aggregated on the surface of Au cores, followed by evacuation of central TiO_2 crystallites (steps 2 and 3, Figure 1). Experiments for tuning Au cores inside TiO_2 nanoreactors were also carried out with two different methods (steps 4 and 5, Figure 1; see the Supporting Information). Flowerlike Au–TiO_2 core–shell structures without central voids (steps I and II, Figure 1) were synthesized with three different methods by varying the reagent concentrations, reaction temperature, and process time (see the Supporting Information). Adsorption and photon-assisted removal of adsorbed dodecanethiol ($C_{12}H_{25}SH$) on the interior Au cores were also conducted (see Supporting Information). The crystallographic structures of the products were determined by X-ray diffraction (XRD; Shimadzu XRD-6000, $Cu_{K\alpha}$). The spatial, morphological, and compositional studies were carried out with field-emission scanning electron microscopy and energy-dispersive X-ray spectroscopy (FESEM/EDX, JSM-6700F), transmission electron microscopy (TEM; JEM-2010F), Fourier-transform infrared spectroscopy (FTIR, KBr method; Bio-Rad FTS 135), and X-ray photoelectron spectroscopy (XPS; AXIS-Hsi, Kratos Analytical).[18,19]

Received: February 2, 2005
Published online: June 13, 2005

Keywords: gold · nanoreactors · nanostructures · photocatalysis

[1] W. Schärtl, *Adv. Mater.* **2000**, *12*, 1899 – 1908.
[2] F. Caruso, *Adv. Mater.* **2001**, *13*, 11 – 22.
[3] C.-J. Zhong, M. M. Maye, *Adv. Mater.* **2001**, *13*, 1507 – 1511.
[4] N. S. Sobal, U. Ebels, H. Möhwald, M. Giersig, *J. Phys. Chem. B* **2003**, *107*, 7351 – 7354.
[5] P. Mulvaney, L. M. Liz-Marzan, M. Giersig, T. Ung, *J. Mater. Chem.* **2000**, *10*, 1259 – 1270.
[6] K. Kamata, Y. Lu, Y. Xia, *J. Am. Chem. Soc.* **2003**, *125*, 2384 – 2385.
[7] Z. Yang, Z. Niu, Y. Lu, Z. Hu, C. C. Han, *Angew. Chem.* **2003**, *115*, 4333 – 4335; *Angew. Chem. Int. Ed.* **2003**, *42*, 1943 – 1945.
[8] H. Gu, R. Zheng, X. Zhang, B. Xu, *J. Am. Chem. Soc.* **2004**, *126*, 5664 – 5665.
[9] P. F. Noble, O. J. Cayre, R. G. Alargova, O. D. Velev, V. N. Paunov, *J. Am. Chem. Soc.* **2004**, *126*, 8092 – 8093.
[10] Y. Yin, R. M. Rioux, C. K. Erdonmez, S. Hughes, G. A. Somorjai, A. P. Alivisatos, *Science* **2004**, *304*, 711 – 714.
[11] H. G. Yang, H. C. Zeng, *J. Phys. Chem. B* **2004**, *108*, 3492 – 3495.
[12] B. Liu, H. C. Zeng, *Small* **2005**, *1*, 566 – 571.
[13] T. Hirakawa, P. V. Kamat, *Langmuir* **2004**, *20*, 5645 – 5647.
[14] Y.-S. Shon, S. M. Gross, B. Dawson, M. Porter, R. W. Murray, *Langmuir* **2000**, *16*, 6555 – 6561.
[15] J. Lukkari, M. Meretoja, I. Kartio, K. Laajalehto, M. Rajamäki, M. Lindström, J. Kankare, *Langmuir* **1999**, *15*, 3529 – 3537.
[16] H. Tada, T. Soejima, S. Ito, H. Kobayashi, *J. Am. Chem. Soc.* **2004**, *126*, 15952 – 15953.
[17] V. Subramanian, E. E. Wolf, P. V. Kamat, *J. Am. Chem. Soc.* **2004**, *126*, 4943 – 4950.
[18] H. G. Yang, H. C. Zeng, *Angew. Chem.* **2004**, *116*, 5318 – 5321; *Angew. Chem. Int. Ed.* **2004**, *43*, 5206 – 5209.
[19] B. Liu, H. C. Zeng, *J. Am. Chem. Soc.* **2004**, *126*, 16744 – 16746.

